CHEMISTRY OF MATERIALS

ARTICLE

pubs.acs.org/cm

# Theoretical Investigation of Grain Size Tuning during Prolonged Bias-Enhanced Nucleation

Maxie Eckert,*[,†] Vincent Mortet,[‡] Liang Zhang,[§] Erik Neyts,[†] Johan Verbeeck,[§] Ken Haenen,[‡] and Annemie Bogaerts[†]

[†]Research Group PLASMANT, Department of Chemistry, University of Antwerp, Universiteitsplein 1, 2610 Antwerp, Belgium,

[‡]Institute for Materials Research (IMO), Hasselt University, Wetenschapspark 1, 3590 Diepenbeek, Belgium and Division IMOMEC, IMEC vzw, Wetenschapspark 1, 3590 Diepenbeek, Belgium

[§]Electron Microscopy for Materials Science (EMAT), University of Antwerp, Groenenborgerlaan 171, 2020 Antwerp, Belgium

**ABSTRACT:** In this paper, the effects of prolonged bias-enhanced nucleation ("prolonged BEN") on the growth mechanisms of diamond are investigated by molecular dynamics (MD) and combined MD-Metropolis Monte Carlo (MD-MMC) simulations. First, cumulative impacts of $C_xH_y^+$ and $H_x^+$ on an a-C:H/nanodiamond composite were simulated; second, nonconsecutive impacts of the dominant ions were simulated in order to understand the observed phenomena in more detail. As stated in the existing literature, the growth of diamond structures during prolonged BEN is a process that takes place below the surface of the growing film. The investigation of the penetration behavior of $C_xH_y^+$ and $H_x^+$ species shows that the carbon-containing ions remain trapped within this amorphous phase where they dominate mechanisms like precipitation of $sp^3$ carbon clusters. The $H^+$ ions, however, penetrate into the crystalline phase at high bias voltages (>100 V), destroying the perfect diamond structure. The experimentally measured reduction of grain sizes at high bias voltage, reported in the literature, might thus be related to penetrating $H^+$ ions. Furthermore, the $C_xH_y^+$ ions are found to be the most efficient sputtering agents, preventing the build up of defective material.

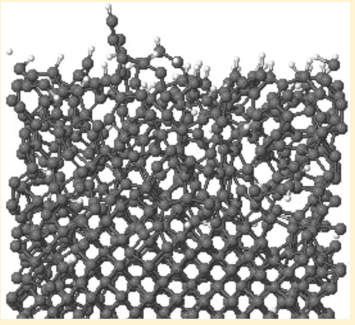

**KEYWORDS:** carbon materials, crystal growth, theory and modeling

## INTRODUCTION

Ultrananocrystalline and nanocrystalline diamond ((U)NCD) thin films have gained widespread research interest due to their unique bulk and surface properties.[1−4] Whereas UNCD consists of spherical, randomly oriented diamond grains with diameters between 3 and 5 nm, NCD is characterized by well-faceted columnar diamond crystals with diameters below 500 nm.[5] The physical properties of the diamond thin films are primarily determined by the size of the diamond grains in the films.[2] Therefore, the capability of tuning the grain sizes when designing the production process is one of the key factors for the applicability of (U)NCD films. Various techniques have been developed to control the grain sizes during chemical vapor deposition (CVD) such as adjusting the substrate temperature and gas pressure[6] and, the most popular, adding noble gases (typically argon) to the methane/hydrogen plasma.[2,7,8] Another technique to control the grain sizes is the application of a substrate bias voltage during the deposition. When applying a constant negative bias voltage during microwave plasma-enhanced CVD (MW PE-CVD) or hot filament CVD, the grain sizes and crystallinity of the films depend strongly on the value of the bias voltage.[9−13] As the decreased grain size at high negative bias voltage is believed to originate from continuous renucleation within the growing film,[9,11,14−18] this technique is often referred to as "prolonged bias-enhanced nucleation"[15−18] (cfr. "bias-enhanced nucleation", BEN, for diamond nucleation at the very first stage of heteroepitaxial diamond growth[19]). In contrast to the adjustment of the deposition conditions such as the gas mixture, prolonged bias-enhanced nucleation enables a good control of the grain sizes within certain regions of the substrate, e.g., at the edges of a diamond-coated tool.[9]

The deposition of diamond thin films under a negative bias, $-V_b$, with typical absolute values up to $V_b$ = 200 V shows that the film morphology and grain size depend strongly on the applied bias voltage. Note that throughout this paper the term "bias voltage" refers to the absolute value $V_b$ of the applied negative bias voltage $-V_b$. In general, two regions of the bias voltage can be distinguished.[10,12,14] As the bias voltage is raised from $V_b$ = 0 V to $V_b$ = 100 V, the crystal size increases and the films become more (100) oriented; as the bias voltage is further raised, the grain size rapidly decreases and the diamond grains become randomly oriented.[12,14]

Growth of the diamond films under a bias voltage is described as precipitation and growth of nanodiamond crystals within an amorphous hydrogenated carbon (a-C:H) matrix such that the resulting film is an a-C:H/nanodiamond composite.[15−17] On the

**Received:** August 30, 2010
**Revised:** December 23, 2010
**Published:** February 23, 2011

atomic level, this a-C:H/nanodiamond composite growth is characterized as a sequence of (i) formation of an a-C:H matrix, (ii) precipitation of $sp^3$ clusters, among which a few perfect diamond crystallites, within the a-C:H matrix, (iii) further growth of the diamond crystallites, (iv) suppression of further growth of the diamond crystallites by the surrounding and growing amorphous a-C:H matrix (encapsulation), and (v) formation of new diamond nuclei within the a-C:H matrix (renucleation).[16,17] Note that in this model, as proposed by Lifshitz et al., diamond nucleation is considered to be a bulk process that occurs ~1−2 nm below the surface; Lifshitz et al. emphasize that if diamond clusters grew on the surface, they would be annihilated or graphitized by the bombarding energetic species.[16]

The prolonged BEN growth is believed to be driven by the energetic $H^+$ and $CH_x^+$ ions that bombard the growing sample,[9,12,20,21] and the key process in prolonged BEN is the subplantation of $CH_x^+$ ions. As the ion bombardment energies increase with negative bias voltage, the ions will be more probable to penetrate into the growing sample. Penetration of the ions is believed to enhance the number of renucleation sites[9,12,20,21] in the form of broken bonds, i.e., dangling bonds. Creation of nucleation sites will inhibit columnar growth of diamond grains,[9,14] as new nuclei will evolve into diamond grains instead of following the van der Drift regime.[4] On the other hand, energetic $H^+$ ions are considered to sputter nondiamond phases and non-(100) planes more efficiently than H atoms do.[9,12,20] If, however, the bias voltage is too high ($V_b$ > 250 V), positive ions may acquire enough energy to destroy the diamond seeds that are formed during the substrate pretreatment and are necessary for diamond film growth, such that no diamond thin films can be grown beyond a certain bias voltage.[11]

In previous research,[6,9,11−13,20] it is shown that the film morphology depends on the applied bias voltage during MW PE-CVD. As the bias voltage is raised from $V_b$ = 0 V to $V_b$ = 100 V, the average grain size slightly increases. Furthermore, the crystallinity, i.e., the ratio of crystalline phase to amorphous phase within the grown films, increases. The deposited films in this bias voltage region exhibit preferential growth orientations, i.e., (110) between $V_b$ = 0 and $V_b$ = 75 V and (100) at higher bias voltages. Once the bias voltage is higher than 140 V, the average grain size decreases and the diamond grains become randomly oriented. In addition, it was observed that the deposition rate of the films is affected by the bias voltage; for low bias voltages, the deposition rate rises slowly, but for the bias voltages between $V_b$ = 100 V and $V_b$ = 300 V, it increases exponentially.[13,20]

In this paper, we report on classical molecular dynamics (MD) simulations in order to understand the dependence of film morphology on the applied bias voltage. In MD, evolution of a system is followed by integration of Newton's equations for the atoms under study, i.e., evolution of the system is followed through time and space. The forces that act on the atoms are derived from a potential function that describes the interactions between the atoms. By performing MD simulations, we investigated the structural changes of an a-C:H/nanodiamond composite after bombardment of 160 species with kinetic energies and relative fluxes that correspond to different bias voltages as reported in the literature.[22] It was shown that as the bias voltage increases, the number of free electrons within the structure is enhanced, which results in an increasing carbon atom incorporation ratio. This explains the experimentally measured deposition rate, which was previously thought to be primarily driven by an increased flux toward the growing sample at higher bias voltage.[22] The MD simulations also support the observation that the crystallinity changes: The radial distribution function (RDF) of the structures, that is, their long-range order, depends on the kinetic energy of the impacting species.

The classical MD simulations enabled us to obtain first insights into the dynamics of the growth of diamond films during prolonged BEN, since "real trajectories" of impacting species on growing samples during CVD are simulated. Nevertheless, relaxation events such as diffusive processes cannot be investigated by means of MD, as the time scale of the MD simulation is limited to at maximum the nanosecond range and relaxation events happen on the microsecond to second time scale.[23] Lifshitz et al. state, however, that some processes during prolonged BEN, like growth of diamond clusters through transformation of amorphous carbon to diamond, are diffusive events.[16] For example, loosely bonded atoms within the amorphous phase move to new diamond positions.[16]

For the description of diffusive and relaxation events, several techniques have been developed. One of the fastest simulation techniques that does not require any assumptions about the reaction mechanisms is the "temperature-accelerated dynamics" (TAD) method, developed by the Los Alamos National Laboratory.[24,25] In essence, during a TAD simulation, infrequent events are accelerated by raising the system temperature. Once an infrequent event occurs, the behavior of the system at the raised temperature is extrapolated to the original (lower) temperature of the system. However, a correct extrapolation requires that all transitions of the considered system obey the harmonic transition state theory.[25] This is not true for our systems under study at relatively high temperatures.

Therefore, in this paper, we apply an algorithm that is based on the Metropolis Monte Carlo (MMC) technique[26] coupled to the MD code,[27,28] such that combined MD-MMC simulations are performed. The MD part deals with the simulation of particle impacts, whereas the MMC part accounts for simulation of relaxation events between two particle impacts onto the growing sample. In contrast to the deterministic MD simulations, in MMC, the system is allowed to evolve based on random displacements, so-called "trial moves". Whether a trial move is accepted or rejected depends on the energy difference that is caused by the trial move. In refs 27 and 28 is was shown that the MMC algorithm reproduces configurations that are obtained by means of MD but at least 10 times faster.

In this paper, mechanisms are investigated that occur when highly energetic ions impact a growing film. These mechanisms will be related to macroscopic observable features during prolonged BEN. By investigating the dynamics of energetic ions, new insights into the growth mechanisms during prolonged BEN will be gained, especially about the role of penetrating $C_xH_y^+$ and $H_x^+$ ions.

Two kinds of simulations are carried out. First, the effect of the bias voltage on the morphology of an a-C:H/nanodiamond composite is investigated by means of combined MD-MMC simulations of consecutive impacts on the growing sample. By means of these simulations, the effects of sequently bombarding species are studied. Second, nonconsecutive impacts are simulated by means of MD, in order to unravel the role of the most important $C_xH_y^+$ and $H_x^+$ ions. In these pure MD simulations, impacts of ions onto the input sample are simulated one by one and the resulting configurations are analyzed individually. Since the species do not bombard the sample cumulatively, the MD

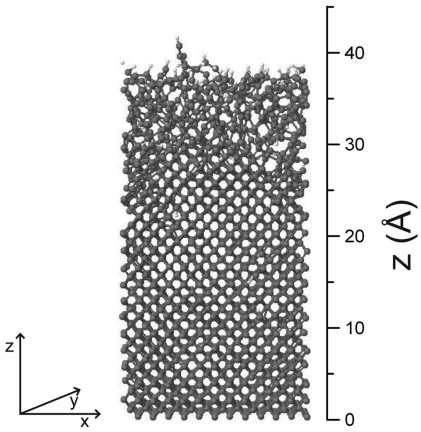


**Figure 1.** Constructed sample utilized as input configuration for this study. The simulation cell embodies 1920 C atoms (dark gray) and 82 H atoms (light gray) and has dimensions of 14.0 Å × 21.0 Å × 41.8 Å. The lower 100 atoms (i.e., two atomic layers) are kept fixed in order to anchor the simulation cell and prevent its translation due to momentum transfer from impacting species. In the $\pm x$ and $\pm y$ directions, periodic boundary conditions are applied.

simulations are independent from each other. Hence, we refer to these simulations as nonconsecutive impacts.

## COMPUTATIONAL DETAILS

**Construction of Bombarded Sample.** For simulation of energetic impacts onto a growing nanocrystalline diamond film, a sample computationally mimicking the growing film was constructed. As proposed by Lifshitz et al., during prolonged BEN, diamond structures precipitate within a dense a-C:H phase which is 1−2 nm thick.[16] Therefore, we constructed computationally an a-C:H/nanodiamond composite, that is, a dense a-C:H layer that shields a diamond phase. As can be seen from Figure 1, the sample is composed of a crystalline part and a distinct amorphous layer that is ∼1.5 nm thick.

This sample was prepared from a perfect diamond (100)2 × 1:2H substrate consisting of 1920 C and 48 H atoms. For obtaining a dense a-C:H phase, hydrogen was incorporated into the diamond substrate by simulating impacts of 60 H atoms onto the perfect diamond (100)2 × 1:2H surface. The kinetic energy of the H atoms was distributed according to the Maxwell distribution with $E_{rms}$ = 60 eV (which corresponds to a substrate bias voltage of 150 V,[22] see text). Taking into account that the hydrogen concentration is known to be 1 order of magnitude higher in the bulk than close to the surface (i.e., the part of the sample that is simulated here), the hydrogen concentration within the simulation cell, $6.7 \times 10^{21}$ cm$^{-3}$, approaches quite well the experimental hydrogen concentration within the bulk of $3 \times 10^{22}$ cm$^{-3}$, as estimated from IR absorption measurements.[29] Regarding the location of the implanted H atoms, the obtained structure fits the theoretical predictions by Michaelson et al.:[30] Although hydrogen atoms are present in the diamond phase, most of the hydrogen is located within the amorphous phase. At the sharp interface between the amorphous and the crystalline phases, the hydrogen concentration is rather low and the hydrogen remains at the amorphous side of the interface. In order to mimic the experimental conditions, a substrate temperature of 1350 K[13] was achieved by applying the Berendsen heat bath.[31]

**Selection of Impacting Species.** The structure as shown in Figure 1 is subject to two different simulation setups: First, cumulative impacts of hydrogen and hydrocarbon ions are simulated onto the input sample. In that manner, growth during prolonged BEN is investigated. Second, nonconsecutive impacts onto the input configuration are simulated for unraveling the underlying mechanisms during prolonged BEN. In order to obtain a better insight into the role of the $C_xH_y^+$ and $H_x^+$ ions, impacts of the ions with the highest fluxes are simulated. In the following, the selection of impacting species is expounded.

**Table 1. Relative Fluxes of Hydrogen Ion and Hydrocarbon Ion Species at Varying Bias Voltages, Derived from the Absolute Fluxes Presented in Ref22 for Typical MW PE-CVD Diamond Growth Conditions, i.e., 0.25% $CH_4$ in a Surplus of $H_2$ at a Gas Pressure of 25 mbar and a Microwave Power of 900 W[a]**

| | | bias voltages | | | | |
|---|---|---|---|---|---|---|
| ion | | 20 V | 50 V | 100 V | 150 V | 200 V |
| $H^+$ | relative flux | | | 0.35 | 0.31 | 0.51 |
| | average energy (eV) | | | 28 | 56 | 84 |
| $H_3^+$ | relative flux | 0.50 | 0.24 | 0.18 | 0.16 | 0.18 |
| | average energy (eV) | 8 | 16 | 20 | 46 | 41 |
| $C^+$ | relative flux | | 0.02 | 0.07 | 0.11 | 0.10 |
| | average energy (eV) | | 19 | 32 | 52 | 82 |
| $CH^+$ | relative flux | | | 0.04 | 0.11 | 0.06 |
| | average energy (eV) | | | 32 | 50 | 73 |
| $CH_2^+$ | relative flux | | 0.05 | 0.10 | 0.08 | 0.03 |
| | average energy (eV) | | 19 | 32 | 46 | 64 |
| $CH_3^+$ | relative flux | 0.30 | 0.37 | 0.12 | 0.05 | 0.02 |
| | average energy (eV) | 10 | 19 | 29 | 38 | 43 |
| $CH_4^+$ | relative flux | | 0.07 | | | |
| | average energy (eV) | | 19 | | | |
| $C_2H^+$ | relative flux | | | | 0.01 | 0.01 |
| | average energy (eV) | | | | 52 | 75 |
| $C_2H_2^+$ | relative flux | | | 0.05 | 0.10 | 0.07 |
| | average energy (eV) | | | 31 | 50 | 72 |
| $C_2H_3^+$ | relative flux | 0.20 | 0.24 | 0.09 | 0.06 | 0.01 |
| | average energy (eV) | 10 | 16 | 31 | 48 | 68 |

[a] The ion energies of the species are distributed according to a Maxwellian distribution; here, the average ion energies are listed.

Kátai et al. succeeded in developing an ion beam mass spectrometer (IBMS) for identification of the most abundant ionic species and measurement of their energy distribution.[32] In ref 22 they present the mass-selective energy distributions of the ions that strike the substrate surface during a BEN process under typical MW PE-CVD diamond growth conditions. Measurements were carried out for bias voltages in the region of $V_b$ = 0−200 V.

On the basis of these fluxes and energy distributions, we identified the species that impact the computational sample during MD and MD-MMC simulations, summarized in Table 1. In this context, "relative flux" refers to the fraction of impacts of a certain species. The relative fluxes of the ions and their energies depend on the bias voltage that is applied, as can be seen from Table 1. At lower bias voltages ($V_b \leq$ 50 V), $H_3^+$ is the dominant bombarding $H_x^+$ ion, and from $V_b$ = 100 V, $H^+$ is the most abundant $H_x^+$ ion arriving at the substrate surface. Regarding the $C_xH_y^+$ species, $CH_3^+$ and $C_2H_3^+$ have the highest fluxes at low bias voltages ($V_b \leq$ 100 V). At bias voltages around 100 V, $C^+$, $CH^+$, $CH_2^+$, and $C_2H_2^+$ become most important. Kátai et al. observe that the average number of hydrogen atoms in $C_xH_y^+$ ions arriving at the surface shows a steep decrease at around $V_b$ = 100 V, which suggests that the energetic collisions in the sheath region, i.e., where the positive ion concentration is high, resulting in dissociation of molecules, become dominant around a bias voltage of 100 V.[22]

According to Kátai et al., most ion energy distributions show a distinct peak at about 15−40% of the bias voltage. As demonstrated in ref 22, the energy of the incident ions is distributed according to a Maxwellian distribution; the energies that are listed in Table 1 are the average ion energies as measured by Kátai et al.[22]

In the consecutive impact simulations, successive impacts of energetic ions onto the sample as shown in Figure 1 are simulated. The kinetic energies and relative frequencies of the species that impact on the sample are chosen as presented in Table 1. In other words, during the consecutive impact simulation, the impacting species are chosen randomly but according to the distribution that is dictated by the relative fluxes, i.e., the frequencies of impacts for each bias voltage can be found in Table 1.

By performing the nonconsecutive impacts, the behavior of both the dominant $C_xH_y^+$ species and the dominant $H_x^+$ species is investigated. In the bias voltage region between $V_b$ = 20 V and $V_b$ = 100 V, $CH_3^+$ is the $C_xH_y^+$ species with the most frequent impacts on the growing sample. At higher bias voltages, $C^+$ is the dominant carbon-containing species. With respect to the hydrogen ions, at bias voltages between $V_b$ = 20 V and $V_b$ = 50 V, $H_3^+$ is the dominant ion, and beyond that bias voltage, $H^+$ is the most important. In other words, these four species are investigated through simulating nonconsecutive impacts on the sample displayed in Figure 1, each within the kinetic energy regions that correspond to the bias voltages at which they are the dominant species, respectively. The $CH_3^+$ and $C^+$ ions are investigated in the energy regions $E_{kin}$ = 10−30 and 40−100 eV, respectively. The $H_3^+$ and $H^+$ ions are investigated in the energy regions 10−20 and 30−100 eV, respectively.

Note that within the MD model, (energetic) ions are represented by (energetic) neutral hydrocarbon species. Indeed, the assumption can be made that all ions are Auger neutralized before reaching the surface, i.e., the ions are neutralized by an emitted electron from the surface.[33] Nevertheless, throughout this paper the impacting species are designated as "ions" in order to avoid confusion.

**Simulation Model and Conditions.** As pointed out above, pure MD simulations are carried out as well as combined MD-MMC simulations. The MD simulation model is utilized for simulation of particle impacts. The MMC part is applied in the case of consecutive impacts for simulation of relaxation events between two successive impacts. In that manner, the term "combined MD-MMC simulation" refers to simulations in which MD and MMC simulations alternate each other (see ref 27 for more details).

Within this model, the interaction between atoms is described by an interatomic potential; for the description of hydrocarbon structures, the well-known Brenner potential is applied.[34] The forces that act on the atoms are derived from the interatomic potential, and these forces determine the new positions and velocities of the atoms. A very extensive description of the MD implementation, including the definition of chemical bonds and the integration scheme, can be found in ref 35.

The impacts of the species are normal to the surface and calculated each during an integration time of 5.0 ps, applying variable time steps between $10^{-7}$ and $10^{-4}$ ps. The initial height of the impacting species above the surface is chosen such that the interaction energy between the surface atoms and the impacting species is negligible; the position in the $\{x,y\}$ plane, i.e., the surface plane, is chosen randomly. The kinetic energy of the impacting species is distributed according to the Maxwell distribution function with values of $E_{rms}$ that vary for the different hydrocarbon species and bias voltages, as presented in Table 1.[22] The rotational and vibrational energies correspond to the typical gas temperature of 2120 K above the substrate surface.[36]

In the case of nonconsecutive impacts, the impact of a particle is followed for 5.0 ps by means of MD, as explained above. During that integration time, an ion impacts the input configuration as shown in Figure 1. Note that for *each* of the nonconsecutive impacts the same input configuration is applied, i.e., the sample structure in Figure 1. After an integration time of 5.0 ps, the resulting structure is analyzed individually.

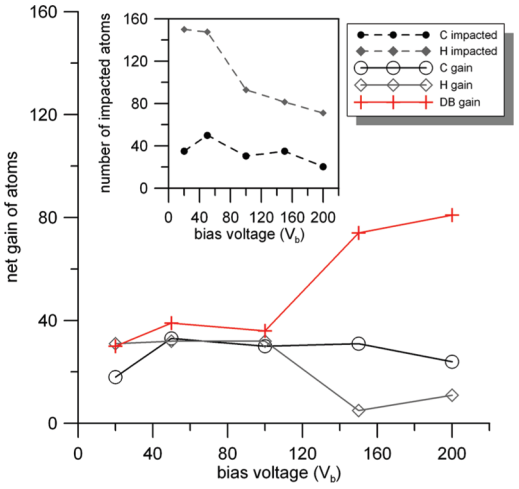


**Figure 2.** Net number of carbon atoms (black line) and hydrogen atoms (gray line) that is incorporated into the sample after 50 consecutive impacts as a function of the applied bias voltage; the red curve shows the gain of free electrons ("dangling bonds", DB). (Inset) Number of carbon and hydrogen atoms that impacted the sample during 50 consecutive impacts, as can be deduced from Table 1.

In case of consecutive impacts, the MD simulation is interrupted after 3.0 ps and the MMC part of the simulation is started. As explained in detail in refs 27 and 28, in the MMC simulation all atoms that are not part of the crystalline phase, i.e., the movers, are allowed to be displaced within a so-called "trial move". As one of the movers is displaced randomly, the potential energy difference caused by that move is calculated. If that difference is equal to or below zero, the move is accepted. Otherwise, the transition probability is calculated, which is defined as the ratio of the occupation probabilities of the original and trial configuration, derived from the Boltzmann distribution function for canonical ensembles.[26] A random number decides then whether the trial move is accepted or not. As the system contains a few hundred movers, the convergence criterion implemented in ref 27—the simulation stops as soon as the number of successive rejected trial moves equals one-half of all trial moves—is not applicable here. Therefore, after 500 000 MMC trial moves, the MMC part of the simulation is stopped. This approach is justified since at that point of the simulation the potential energy fluctuates with only a small amplitude (∼0.1 eV). After the MMC simulation, the system is again allowed to evolve according to the MD code for 2.0 ps with the Berendsen heat bath turned on such that the system is cooled back to 1350 K. As soon as this MD-MMC cycle is finished, the resulting configuration is subject to a new energetic impact, where the same procedure is followed.

## RESULTS AND DISCUSSION

**Consecutive Impacts.** For investigating the effect of the bias voltage on the a-C:H/nanodiamond composites, we simulated 50 cumulative impacts on the sample structure (see Figure 1). According to Table 1, the relative fluxes and energies of the impacting species are varied in order to simulate different bias voltages, i.e., five simulation conditions that correspond to bias voltages in the region $V_b$ = 20−200 V are applied.

When rendering the resulting configurations from 50 consecutive impacts into 3D chemical structures analogous to


dx.doi.org/10.1021/cm102481y |*Chem. Mater.* 2011, 23, 1414–1423

Figure 1, no obvious differences from the input sample, as displayed in Figure 1, can be seen: The bombarded samples still consist of an amorphous phase and a crystalline phase that are divided by a sharp interface. The structural changes are thus more subtle, i.e., a closer look on the atomic level is required in order to gain insights into the structural changes due to the bias voltage.

In the following, the effects of the bias voltage on the morphology will be expounded, including the atomic composition of the films, the distribution of the carbon coordination numbers, and the crystallinity.

*Composition of the Films.* In the bias voltage region $V_b$ = 20−150 V, the composition of the *crystalline phase* was found to be invariant after 50 cumulative impacts, i.e., the number of carbon and hydrogen atoms is not affected. At $V_b$ = 200 V, however, a slight change of the composition can be observed: Four hydrogen atoms have penetrated the crystalline phase. At the bias voltage $V_b$ = 200 V, almost 10% of the impacts resulted thus in penetration of atoms into the crystalline phase. As will be explained below, the range of penetrating ions is highly dependent on their kinetic energy, i.e., the applied bias voltage.

In Figure 2, the net gain of hydrogen and carbon atoms after 50 consecutive impacts is shown. At maximum the resulting structure contains 33 additional C atoms (at $V_b$ = 50 V) and at minimum only 18 additional C atoms (at $V_b$ = 20 V). The net gain of H atoms is the highest at bias voltages between $V_b$ = 20 V and $V_b$ = 100 V (∼31 additional H atoms), and the net gain of H atoms is lowest for the highest bias voltages (at $V_b$ = 150 and 200 V, 5 and 11 additional H atoms, respectively). Note that comparing the incorporation of hydrogen and carbon atoms as displayed in Figure 2 and the experimentally measured growth rate at different bias voltages[13,20] is not straightforward. Indeed, in the MD-MMC simulations, the enhanced absolute flux of species toward the surface at higher bias voltages, which is observed experimentally,[22] cannot be taken into account as the MMC part of the code is not coupled to a time scale. Nevertheless, from Figure 2, more insight into the enhanced growth rate with increasing bias voltage can be attained, as explained below.

The inset in Figure 2 shows the absolute numbers of C and H atoms that have bombarded the input sample during 50 simulated impacts. From Figure 2 it can be seen that the number of implanted H atoms is much lower than one would expect from the number of impacted H atoms. This might be due to reflection of hydrogen-containing ions and/or removal of H atoms from the sample by impacting ions. These mechanisms will be discussed in more detail below; as will be shown below, at high bias voltages, the $C_xH_y^+$ species have a very high hydrogen sputter efficiency.

Furthermore, from the inset within Figure 2 it can be deduced that the number of C atoms that impacts on the sample at $V_b$ = 50 V is more than twice the number of C atoms that impacts on the sample at $V_b$ = 200 V. Nevertheless, the number of implanted C atoms only slightly decreases when the bias voltage is raised from $V_b$ = 50 V to $V_b$ = 200 V. This enhanced C incorporation ratio, i.e., the ratio of incorporated to impacted C atoms, might be explained by the changes of the sample structure due to the bombarding ions: The higher the kinetic energy of the impacting ions, the more bonds will be broken within the bombarded films, that is, the more reactive sites will be created. This can indeed be seen in Figure 2 (red curve). Hence, the exponential increase of the growth rate at high bias voltages is not only due to an increased absolute flux toward the surface but also due to activation of the growing film, resulting in a higher incorporation probability of impacting ions.

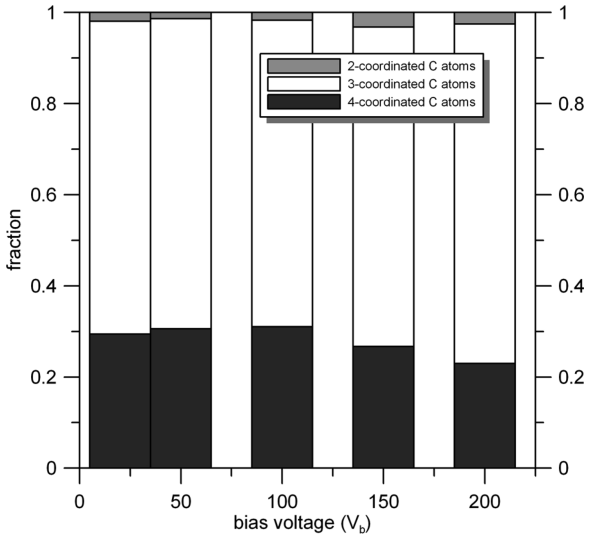


**Figure 3.** Distribution of the coordination numbers of the carbon atoms within the amorphous phase of the bombarded sample, i.e., the upper 17 Å of the samples, after 50 consecutive impacts. On the *x* axis, the bias voltage is displayed that corresponds to the relative fluxes and kinetic energies presented in Table 1.

In ref 13 we concluded from pure MD simulations that the number of free electrons within the film increases as the bias voltage increases, very similar to the results presented in Figure 2. By applying the MMC algorithm, the samples are allowed to relax between two successive impacts. However, we still observe a high number of dangling bonds within the films at high bias voltages. It can thus be concluded that the damage caused by energetic ions is not easily restored, implying that highly energetic ions can cause structural changes within the growing films that determine the resulting film morphology.

*Carbon Coordination within the Bombarded Films.* In our MD simulations, the hybridization of atoms cannot be determined, as it is a classical model. Therefore, instead of their hybridization, the coordination numbers of the atoms are determined. Those coordination numbers are associated with the hybridizations, i.e., four-, three-, and two-coordinated carbon atoms correspond to $sp^3$-, $sp^2$-, and sp-hybridized carbon atoms.

The coordination of the atoms within the *crystalline phase* is not altered significantly for the bias voltage region $V_b$ = 20−100 V. At the highest bias voltages, i.e., at $V_b$ = 150 and 200 V, a slight shift toward three coordination of the carbon atoms can be observed: ∼10 carbon atoms change from four coordination to three coordination. It can thus be stated that only at very high bias voltages the crystalline phase is affected by incoming ions. In that manner, diamond crystallites that are formed during film growth can be damaged, although they are shielded by an amorphous layer. Below, it will be shown that only ions with the highest kinetic energy have sufficient penetration depths for affecting the crystalline phase.

In the *amorphous phase* of the samples, however, we can see greater differences between the samples: The number of four-coordinated carbon atoms within the amorphous part of the samples varies between 136 (at $V_b$ = 200 V) and 184 (at $V_b$ = 100 V). In Figure 3, the distribution of the carbon coordination within the amorphous phase can be found. For all conditions,


dx.doi.org/10.1021/cm102481y |*Chem. Mater.* 2011, 23, 1414–1423

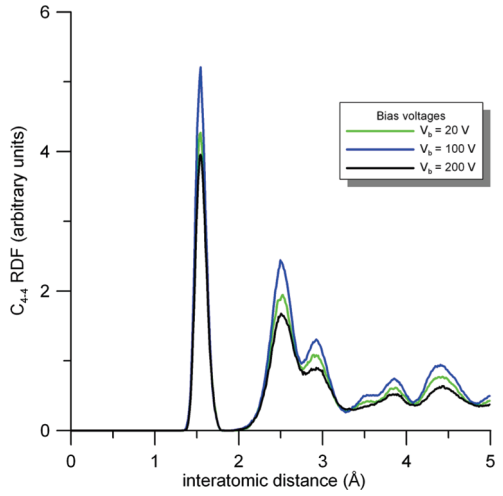


**Figure 4.** Normalized radial distribution functions (RDFs) of the four-coordinated carbon atoms within the bombarded samples. The normalized $C_{4-4}$ RDF measures the probability of finding a four-coordinated C atom at a certain interatomic distance from any other four-coordinated C atom, relative to the same probability in an ideal gas at the same overall number density. For the investigation of the evolution of the amorphous part of the sample, only the upper parts of the samples are taken into account, i.e., the upper 17 Å. For clarity reasons, only the RDFs after 50 consecutive impacts at 20 (green curve), 100 (blue curve), and 200 V (black curve) are shown. The RDFs for the samples at 50 and 150 V lie between the lowest and the highest curve.

most of the carbon atoms within the amorphous phase are three coordinated. At maximum, the amorphous phase contains 31% four-coordinated atoms (at $V_b$ = 100 V) and at minimum only 22% four-coordinated atoms (at $V_b$ = 200 V).

As described by Lifshitz et al., formation of diamond clusters starts with precipitation of $sp^3$-hybridized carbon clusters within an a-C:H phase.[15−17] From Figure 3 we can see that at lower bias voltages ($V_b$ = 20−100 V) formation of four-coordinated carbon atoms is more probable than at higher bias voltages. As explained above, at higher bias voltages the number of free electrons is much higher than at lower bias voltages, which might be caused by energetic ions that break bonds within the film as they impact the sample. The shift to lower coordination numbers of the carbon atoms confirms the assumption that energetic ions break bonds within the structure.

In conclusion, precipitation of $sp^3$-hybridized clusters can be expected to be suppressed at bias voltages as high as $V_b$ = 150−200 V due to the bond breaking of four-coordinated carbon atoms.

*Crystallinity of the Films.* In the previous subsection the fraction of four-coordinated carbon atoms was related to the ability of $sp^3$ precipitation within the amorphous phase. In this subsection, we go into more detail about the formation of long-range order of four-coordinated carbon atoms, i.e., the crystallinity within the samples. As a measure of the long-range order within the samples, the RDFs of the samples were calculated. The RDFs of crystalline materials exhibit well-defined peaks and valleys that represent the periodicity of interatomic distances within the solid. In contrast, amorphous materials are characterized by RDFs with less pronounced or even absent peaks, especially for the longer length scale.

In Figure 4 the RDFs of the amorphous phase of three samples can be found. As the bias voltage is increased from $V_b$ = 20 V to $V_b$ = 100 V, it can be observed that the RDF curve exhibits more pronounced peaks. Note that this increase is more striking than the increase of the fraction of four-coordinated carbon atoms (see Figure 3). As the bias voltage is further increased to $V_b$ = 200 V, the peaks of the RDF decreases again and the long-range order is much less pronounced. Figure 4 thus indicates that there is a certain optimum value for the formation of crystalline structures within the amorphous phase, in agreement with Lifshitz et al.:[16] Around $V_b$ = 100 V, the long-range order, i.e., at a later stage of growth the crystalline phase, of the film is the highest.

The increase in crystallinity as the bias voltage is raised, followed by its decrease at bias voltages higher than 130 V, was observed experimentally by several authors.[12−14] Hence, our simulations reflect the morphology changes that are measured experimentally and the assumption that the bias voltage contributes to precipitation of $sp^3$-hybridized carbon clusters that can evolve into diamond crystallites.

In ref 13 calculated RDFs were presented as obtained by pure MD simulations. Note that they differ somewhat from the curves in Figure 4: In the case of pure MD simulations,[13] the RDF curves of the samples bombarded at bias voltages lower than 100 V were found to coincide; however, for the sample bombarded at $V_b$ = 200 V, the long-range order has almost disappeared. These differences can again be explained by the fact that in the current MD-MMC simulations relaxation events are taken into account; hence, some of the disturbances caused by energetic ions (see above) are restored. This effect results in an enhanced crystallinity within the region $V_b$ = 100−200 V. Note that, however, not all created defects are restored: As can be seen from the RDF of the sample at the highest bias voltage (Figure 4), the long-range order diminishes. This is in agreement with the presence of dangling bonds at high bias voltages (see above).

In the Appendix, one can find a table that summarizes the observations as expounded in this subsection. This table might improve readability of the next subsection, where the underlying mechanisms of growth during prolonged BEN are unraveled and related to the observations.

**Nonconsecutive Impacts.** In the following subsections we attempt to unravel the reaction mechanisms in detail that occur when energetic species impact on the sample structure (see Figure 1). For a better understanding of the growth mechanisms during prolonged BEN, nonconsecutive impacts of the most important $C_xH_y^+$ and $H_x^+$ species were simulated and analyzed individually. By investigating both the $C_xH_y^+$ and the $H_x^+$ ions that account for the most frequent impacts on the growing film, the different role of the hydrocarbon ions and hydrogen ions is examined. As pointed out in the Introduction, the $C_xH_y^+$ and $H_x^+$ ions might play different roles during film growth and development of the morphology.[9,12,20]

As can be deduced from Table 1, for the bias voltage region $V_b$ = 20−100 V, $CH_3^+$ ions account for the most frequent $C_xH_y^+$ impacts during growth of the film, whereas beyond $V_b$ = 100 V, the $C^+$ ion is the dominant $C_xH_y^+$ bombarding ion. The $H_3^+$ ion is the dominant impacting ion within the bias voltage region between $V_b$ = 20 V and $V_b$ = 50 V, whereas at higher bias voltages $H^+$ becomes dominant. Note that at lower bias voltages molecular ions dominate the flux to the growing film, whereas at higher bias voltages atomic ions are more important. As will be discussed below, this affects the behavior of the impacting species.

Three basic mechanisms are observed when $C_xH_y^+$ and $H_x^+$ ions impact the sample structure: sticking (including subsurface

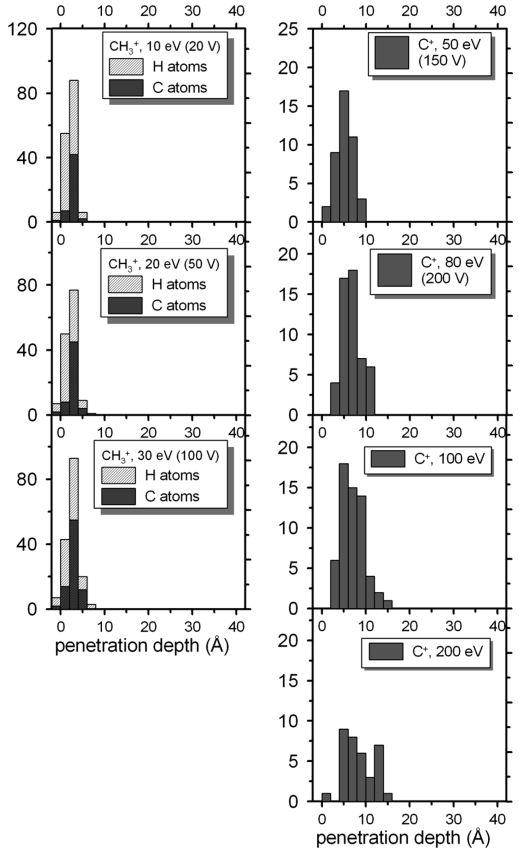


**Figure 5.** Histograms of the penetration depths of atoms originating from the impacting $C_xH_y^+$ ions, i.e., $CH_3^+$ (left) and $C^+$ (right). The penetration depth is defined as the distance in the negative direction from the highest atomic position within the input sample (see Figure 1). For each investigated kinetic energy (and corresponding bias voltage), 100 nonconsecutive impacts on the sample structure were analyzed. The penetration depths for C and H atoms originating from impacting $CH_3^+$ ions are investigated within the bias voltage region $V_b$ = 20−100 V, corresponding to kinetic energies between 10 and 30 eV. For the bias voltage range $V_b$ = 150−200 V, the penetration behavior of $C^+$ was examined, corresponding to kinetic energies of 50 and 80 eV, respectively. In addition, the penetration depths of $C^+$ ions with kinetic energies as high as 100 and 200 eV were investigated in order to gain more insight into the penetration behavior of $C^+$ ions. As can be estimated by extrapolation, these kinetic energies would correspond to a bias voltage around 400 V, which is far beyond the experimentally applied bias voltages.

implantation, the so-called "subplantation") of the impacting species, reflection at the sample, and sputtering (including both chemical and physical sputtering). In the following, the effect of the bias voltage on addition of atoms through sticking and subplantation and on removal of atoms from the bombarded sample through sputtering is discussed in detail. In the Appendix, the distribution of the mechanisms as a function of bias voltage can be found.

*Sticking and Penetration Behavior of Impacting Ions.* It is very probable that the impacting $C_xH_y^+$ ions form bonds to the sample: The sticking coefficient equals ∼0.5 or more within the studied bias voltage region. Note that here "sticking coefficient" refers to the fraction of all implemented ions, i.e., both by chemisorption at the surface and by subplantation.

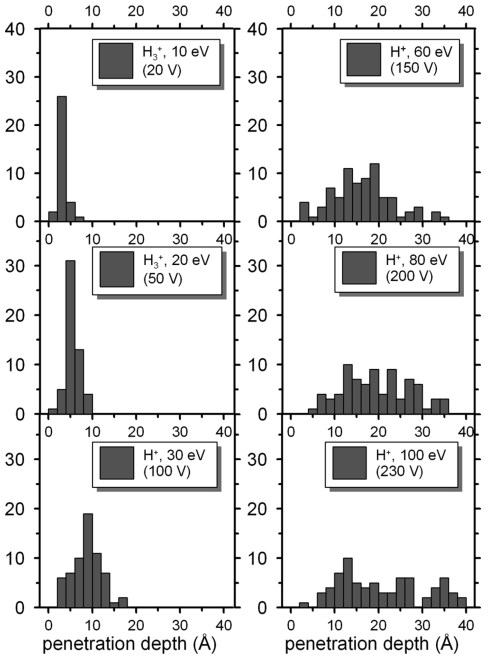


**Figure 6.** Histograms of the penetration depths of atoms originating from the impacting $H_x^+$ ions, i.e., $H_3^+$ and $H^+$. The penetration depth is defined as the distance in the negative direction from the highest atomic position within the input sample (see Figure 1). For each investigated kinetic energy (and corresponding bias voltage), 100 nonconsecutive impacts on the sample structure were analyzed. The penetration depths for H atoms originating from impacting $H_3^+$ ions are investigated within the bias voltage region $V_b$ = 20−50 V, corresponding to kinetic energies of 10 and 20 eV. For the bias voltage range $V_b$ = 100−200 V, the penetration behavior of $H^+$ was examined, corresponding to kinetic energies between 30 and 100 eV.

For the $CH_3^+$ species (investigated at kinetic energies that correspond to bias voltages $V_b \leq 100$ V), sticking is less probable than that for the $C^+$ ion (important at bias voltages $V_b > 100$ V); the sticking probabilities are ∼0.5 and ∼0.9 for $CH_3^+$ and $C^+$, respectively. The lower reactivity of the $CH_3^+$ ions can be explained by the fact that the hydrogen atoms within the $CH_3^+$ ion shield the carbon atom from reactive sites at the sample surface, which lowers the sticking probability.[35] Furthermore, a $CH_3^+$ ion has to fragment into atoms before the atoms can penetrate separately the sample surface,[37] such that only the fragmented ions have a chance to be subsurface implemented. The penetration probability of a molecular ion will thus be lower than that for atomic ions.

The same observation can be made for the $H_x^+$ ions: The sticking and penetration probability of the $H_3^+$ ions (important in the bias voltage region $V_b$ = 20−50 V) is ∼0.3−0.4, whereas the sticking coefficient of the $H^+$ ion (important at bias substrate voltages $V_b \geq 100$ V) is ∼0.6−0.8. As is true for the $CH_3^+$ ions, $H_3^+$ ions have to fragment before they can penetrate the sample or form bonds to reactive sites at the sample surface.

In order to gain more insight into the penetration behavior of the ions that are incorporated in the film, we calculated the penetration depths of the implemented species, see Figures 5 and 6. It is clear from Figure 5 that the $CH_3^+$ ions remain at or close to the surface. The $C^+$ ions with kinetic energies corresponding to bias voltages $V_b$ = 150−200 V can penetrate much deeper (i.e.,

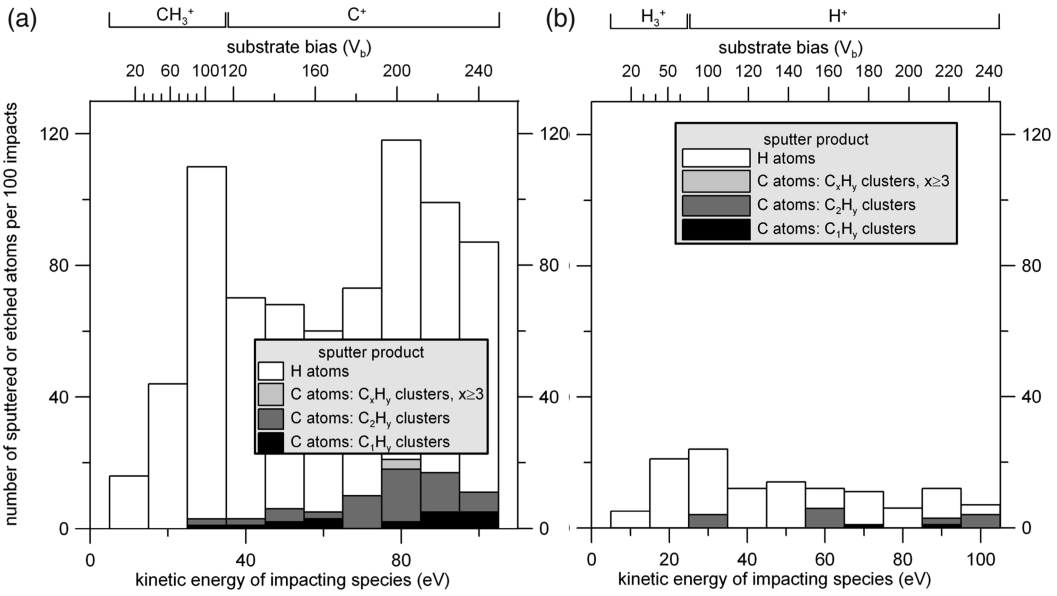


**Figure 7.** Number of atoms removed by impacting $C_xH_y^+$ ions (a) and $H_x^+$ ions (b), summed over 100 nonconsecutive impacts. The upper *x* axes again indicate the bias voltages that correspond to the kinetic energies (lower *x* axes) which are examined as well as the dominant impacting ions, i.e., the species that are investigated within a certain bias voltage region. Note that the removed carbon atoms are grouped according to the clusters that desorb. However, the *y* axes indicate the *total number of removed atoms* and not the number of $C_xH_y$ clusters that desorb from the sample.

up to roughly 10 Å); however, nearly all $C^+$ ions still remain within the amorphous phase of the sample. In contrast to the behavior of the $C_xH_y^+$ ions, the $H_x^+$ ions penetrate much deeper, see Figure 6: Hydrogen atoms interact much weaker with the carbon atoms of the bombarded sample due to their small size and mass.[38] At the bias voltage $V_b$ = 100 V (corresponding kinetic energy of the $H^+$ ions: 30 eV, see Figure 6), the hydrogen atoms start to penetrate into the crystalline part of the sample. At the bias voltage $V_b$ = 150 V, more than one-half of the $H^+$ ions reach the crystalline phase of the sample. The higher the kinetic energy of the $H^+$ ions, the more the distribution of the penetration depth shifts to greater depths and the more it spreads out.

These observations are in agreement with the results presented in the previous subsection for consecutive impacts: At the highest bias voltage, four hydrogen atoms have penetrated the crystalline phase (see above). However, for the other bias voltages, no penetration into the crystalline phase is observed. This might be explained by the fact that the fraction of impacting $H^+$ ions is significantly lower at $V_b$ = 100−150 V than at $V_b$ = 200 V (see Table 1).

As observed experimentally[6,9,11−13,20] and argued in the previous subsection, at high bias voltages the morphology of the deposited films changes, i.e., the crystallinity decreases and the diamond grain sizes are reduced (see above). The reduction of the grain sizes might be related to the behavior of the impacting hydrogen ions: At bias voltages $V_b \leq$ 100 V, very few hydrogen ions reach the crystalline phase and the majority are trapped in the amorphous phase of the sample. The same applies to the $C_xH_y^+$ ions. Hence, at lower bias voltages, the crystalline phase is not affected. At high bias voltages, i.e., beyond $V_b$ = 100 V, however, the $H^+$ ions can penetrate the diamond phase; indeed, they have enough energy to destroy grown diamond structures. This was indeed observed for consecutive impacts at $V_b$ = 200 V (see above).

The carbon-containing ions will still be trapped in the amorphous part of the sample at bias voltages higher than $V_b$ = 100 V, and as mentioned above, the implementation probability is higher for $C^+$ ions than for $H^+$ ions. It is thus very likely that the processes that occur within the amorphous phase of the sample, e.g., precipitation of $sp^3$ clusters and bond breaking, are dominated by impacting atoms originating from carbon-containing ions. The decrease of the crystallinity at bias voltages higher than $V_b$ = 100 V is, however, very probable to be caused by impacting hydrogen atoms that penetrate the crystalline phase and destroy the crystal structure.

*Sputtering Behavior of Impacting Ions.* In this subsection, we do not go into much detail about the different sputter mechanisms; we rather report the *total sputter yield*, since we are interested in the efficiency with which atoms are removed from the growing films. Removal of atoms will be termed "sputtering", summarizing chemical and physical sputtering.

In Figure 7a and 7b the yields of the individual sputter products are displayed for the impacting $C_xH_y^+$ and $H_x^+$ species, respectively. Note that the sputter yield for the $H_x^+$ species is much lower than that for the $C_xH_y^+$ species for all bias voltages (i.e., a factor of 2 lower at $V_b$ = 40 V, up to a factor of 20 lower at $V_b$ = 200 V). It appears that the flux of hydrogen ions does not compensate for the prominent role of the $C_xH_y^+$ ions in removing atoms from the sample: At $V_b$ = 40 V, the ratio of the $H^+$ flux to the $CH_3^+$ flux is ∼0.7; at $V_b$ = 200 V, the ratio of the $H^+$ flux to $C^+$ flux equals ∼5.[22] Compare this to the sputter yield of the carbon-containing ions, which is 2−20 times higher than the yield of the $H_x^+$ ions.

In conclusion, the $C_xH_y^+$ species might play a more important role in removing amorphous material from the growing film than the $H_x^+$ ions, in contrast to the assumption that at high bias voltages $H^+$ is an important sputtering species which prevents the build up of defective material.[12]


dx.doi.org/10.1021/cm102481y |*Chem. Mater.* 2011, 23, 1414–1423

## CONCLUSION

In this paper, we studied the effects of prolonged bias-enhanced nucleation on the growth mechanisms of diamond. In order to obtain better insight into the effect of a negative bias voltage at the substrate during growth of (ultra)nanocrystalline diamond on the atomic level, two kinds of simulations were performed: First, cumulative impacts of several different $C_xH_y^+$ and $H_x^+$ ions on an a-C:H/nanodiamond composite were simulated; second, nonconsecutive impacts of the dominant ions were simulated in order to better understand the observed phenomena. The investigations were performed by means of MD (for the nonconsecutive impacts) and combined MD-MMC (for the consecutive) simulations. The impacting species and their kinetic energies were selected based on experimental measurements reported in the literature.

First, it was found not only that the experimentally observed exponential increase of the growth rate at high bias voltages is caused by an increased flux of species to the growing film at higher bias voltages but that the growing film will also be activated by formation of reactive sites, i.e., free electrons, such that the probability of impacting ions to be implanted increases with increasing bias voltage.

In agreement with the existing literature, a bias voltage on the substrate enhances formation of a long-range order, i.e., the crystallinity, as was shown by the calculated RDFs of the samples. If, however, the bias voltage is raised to values beyond $V_b$ = 100 V, bonds within the bombarded samples are broken, suppressing formation of $sp^3$ clusters and thwarting formation of diamond crystallites, again in agreement with experimental findings.

As stated in the existing literature, growth of diamond structures during prolonged BEN is a bulk process, i.e., a process that takes place below the surface of the growing film. Investigation of the penetration behavior of $C_xH_y^+$ and $H_x^+$ species shows the following: It is very improbable that carbon-containing ions penetrate into the crystalline phase that is shielded by an a-C:H layer with a thickness of 1−2 nm; instead, they remain trapped within the amorphous phase. The $H^+$ ions, however, penetrate much deeper. At high bias voltages ($V_b$ > 100 V) they gain enough kinetic energy to penetrate into the crystalline phase, destroying the perfect diamond structure. The experimentally measured reduction of grain sizes at high bias voltage might thus be related to penetrating $H^+$ ions. On the other hand, the $C_xH_y^+$ ions are trapped within the amorphous phase, where they dominate mechanisms like precipitation of $sp^3$ carbon clusters and bond breaking.

Another observation regarding the different role of hydrogen- and carbon-containing ions was made: In contrast to the assumption that hydrogen ions are the most efficient sputtering species, we found that the $C_xH_y^+$ ions are much more efficient in removing atoms from the growing sample, which is even not compensated by the higher flux of hydrogen ions to the growing sample. In other words, the $C_xH_y^+$ ions are, in absolute terms, the most efficient sputtering agents, preventing the build up of defective material.

These deeper insights into the growth mechanisms during prolonged BEN encourage the experimental application of a substrate bias voltage during the growth of nanodiamond films, enabling a better grain size tuning.

## APPENDIX

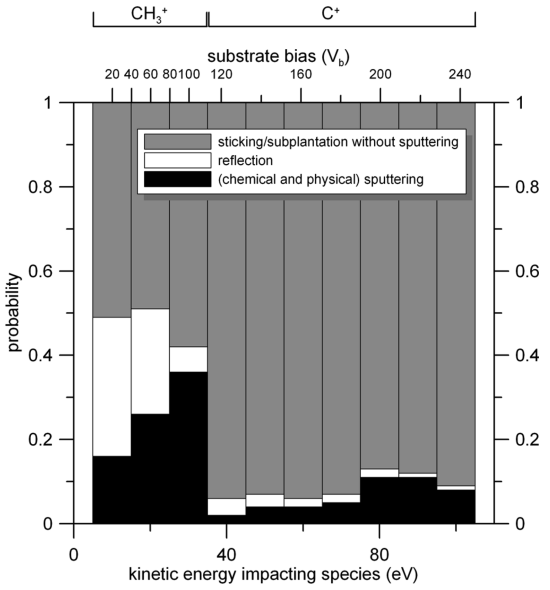


**Figure 8.** Overview of the reaction mechanisms of the dominant $C_xH_y^+$ ions impacting the sample structure. In the bias voltage region $V_b$ = 20−100 V (upper *x* axis), 100 impacts of $CH_3^+$ ions with corresponding kinetic energies (lower *x* baxis) are analyzed; at the higher bias voltage region and kinetic energies, the behavior of the $C^+$ ions is investigated. Above the upper *x* axis, the dominant $C_xH_y^+$ ions are indicated. The probabilities are calculated as the frequencies of occurrence as observed for the 100 nonconsecutive impacts.

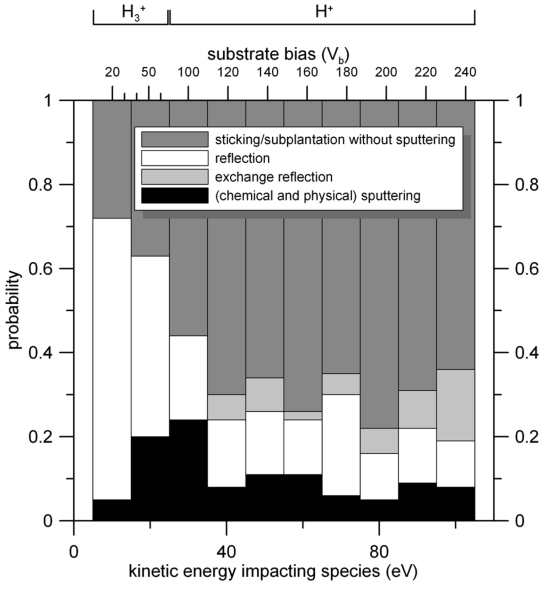


**Figure 9.** Overview of the reaction mechanisms of the dominant $H_x^+$ ions impacting the sample structure. In the bias voltage region $V_b$ = 20−50 V (upper *x* axis), 100 impacts of $H_3^+$ ions with corresponding kinetic energies (lower *x* axis) are analyzed; at the higher bias voltage region and kinetic energies, the behavior of the $H^+$ ions is investigated. Above the upper *x* axis, the dominant $H_x^+$ ions are indicated. The probabilities are calculated as the frequencies of occurrence as observed for the 100 nonconsecutive impacts.

**Table 2. Summary of the Observations Made When Simulating Consecutive Particle Impacts (see the Results section)**

| | bias voltage (region) | | |
|---|---|---|---|
| | 20−100 V | 150 V | 200 V |
| | crystalline phase | | |
| gain C atoms | | | |
| gain H atoms | | | 4 penetrated H atoms |
| C coordination | | slight shift from 4 to 3 coordination | |
| | amorphous phase | | |
| gain H atoms | ∼31 | 5 | 11 |
| gain C atoms | C incorporation ratio increases as $V_b$ increases | | |
| dangling bonds | number of DB's increases as $V_b$ increases | | |
| C coordination | ∼30% 4-coordination | 26% 4-coordination | 22% 4-coordination |
| crystallinity | increases with $V_b$ | decreases with increasing $V_b$ | |

## AUTHOR INFORMATION


### Corresponding Author

*Phone: +32 32 65 23 82. Fax: +32 32 65 23 76. E-mail: maxie.eckert@ua.ac.be.


## ACKNOWLEDGMENT


M.E. is indebted to the Institute for the Promotion of Innovation through Science and Technology in Flanders (IWT-Vlaanderen) for financial support. E.N. acknowledges financial support from the Fund for Scientific Research-Flanders (FWO). J.V. acknowledges financial support from the European Union under the Framework 6 program under a contract for an Integrated Infrastructure Initiative, Reference 026019 ESTEEM. This work was financially supported by the IAP-P6/42 project Quantum Effects in Clusters and Nanowires and the Fund for Scientific Research-Flanders (FWO). The calculation support of the core facility CALCUA, provided by the University of Antwerp, is gratefully acknowledged.


## REFERENCES


(1) Das, D.; Singh, R. N. *Int. Mater. Rev.* **2007**, *52*, 29–64.
(2) Gruen, D. M. *Annu. Rev. Mater. Sci.* **1999**, *29*, 211–259.
(3) May, P. W. *Philos. Trans. R. Soc. London A* **2000**, *358*, 473–495.
(4) Williams, O. A.; Nesládek, M.; Daenen, M.; Michaelson, S.; Hoffman, A.; Osawa, E.; Haenen, K.; Jackman, R. B. *Diamond Relat. Mater.* **2008**, *17*, 1080–1088.
(5) Williams, O. A.; Daenen, M.; D'Haen, J.; Haenen, K.; Maes, J.; Moshchalkov, V. V.; Nesládek, M.; Gruen, D. M. *Diamond Relat. Mater.* **2006**, *15*, 654–658.
(6) Kang, M.-S.; Lee, W.-S.; Baik, Y.-J. *Thin Solid Films* **2001**, *398*−*399*, 175–179.
(7) Zhou, D.; Gruen, D. M.; Qin, L. C.; McCauley, T. G.; Krauss, A. R. *J. Appl. Phys.* **1998**, *84*, 1981–1989.
(8) Uppireddi, K.; Weiner, B. R.; Morell, G. *Diamond Relat. Mater.* **2008**, *17*, 55–59.
(9) Park, J.-K.; Lee, W.-S.; Baik, Y.-J.; Chae, K.-W. *Diamond Relat. Mater.* **2003**, *12*, 1657–1662.
(10) Schreck, M.; Baur, T.; Fehling, R.; Muller, M.; Stritzker, B.; Bergmaier, A.; Dollinger, G. *Diamond Relat. Mater.* **1998**, *7*, 293–298.
(11) Jiang, N.; Sugimoto, K.; Eguchi, K.; Inaoka, T.; Shintani, Y.; Makita, H.; Hatta, A.; Hiraki, A. *J. Cryst. Growth* **2001**, *222*, 591–594.
(12) Yang, T.-S.; Lai, J.-Y.; Wong, M.-S.; Cheng, C.-L. *J. Appl. Phys.* **2002**, *92*, 2133–2138.
(13) Mortet, V.; Zhang, L.; Eckert, M.; D'Haen, J.; Soltani, A.; Douhŕet, O.; Moreau, M.; Troadec, D.; Neyts, E.; De Jaeger, J. C.; Verbeeck, J.; Bogaerts, A.; Van Tendeloo, G.; Haenen, K.; Wagner, P. *Adv. Funct. Mater.* Submitted for publication.
(14) Gu, C. Z.; Jiang, X. *J. Appl. Phys.* **2000**, *88*, 1788–1793.
(15) Zhou, X. T.; Li, Q.; Meng, F. Y.; Bello, I.; Lee, C. S.; Lee, S. T.; Lifshitz, Y. *Appl. Phys. Lett.* **2002**, *80*, 3307–3309.
(16) Lifshitz, Y.; Köhler, T.; Frauenheim, T.; Guzmann, I.; Hoffman, A.; Zhang, R. Q.; Zhou, X. T.; Lee, S. T. *Science* **2002**, *297*, 1531–1533.
(17) Zhou, X. T.; Meng, X. M.; Meng, F. Y.; Li, Q.; Bello, I.; Zhang, W. J.; Lee, C. S.; Lee, S. T.; Lifshitz, Y. *Diamond Relat. Mater.* **2003**, *12*, 1640–1646.
(18) Lifshitz, Y.; Lee, C. H.; Wu, Y.; Zhang, W. J.; Bello, I.; Lee, S. T. *Appl. Phys. Lett.* **2006**, *88*, 243114.
(19) Tshepe, T.; Prins, J. F.; Hocha, M. J. R. *Diamond Relat. Mater.* **1999**, *8*, 1508–1510.
(20) Yang, T. S.; Lai, J. Y.; Wong, M. S. *J. Appl. Phys.* **2002**, *92*, 4912–4917.
(21) Marton, M.; Izák, T.; Veselý, M.; Vojs, M.; Michalka, M.; Bruncko, J. *Vacuum* **2008**, *82*, 154–157.
(22) Kátai, S.; Tass, Z.; Hárs, G.; Deák, P. *J. Appl. Phys.* **1999**, *86*, 5549–5555.
(23) Doll, J. D.; Voter, A. F. *Annu. Rev. Phys. Chem.* **1987**, *38*, 413–431.
(24) Voter, A. F.; Montalenti, F.; Germann, T. C. *Annu. Rev. Mater. Sci.* **2002**, *32*, 321–346.
(25) Sorensen, M. R.; Voter, A. F. *J. Chem. Phys.* **2000**, *112*, 9599–9606.
(26) Metropolis, N.; Rosenbluth, A. W.; Rosenbluth, M. N.; Teller, A. H.; Teller, E. *J. Chem. Phys.* **1953**, *21*, 1087–1092.
(27) Eckert, M.; Neyts, E.; Bogaerts, A. *CrystEngComm* **2009**, *11*, 1597–1608.
(28) Eckert, M.; Neyts, E.; Bogaerts, A. *Cryst. Growth Des.* **2010**, *10*, 3005–3021.
(29) Mortet, V.; Zhang, L.; Eckert, M.; Soltani, A.; D'Haen, J.; Douhŕet, O.; Moreau, M.; Osswald, S.; Neyts, E.; Troadec, D.; Wagner, P.; Bogaerts, A.; Van Tendeloo, G.; Haenen, K.; Wagner, P. *Mater. Res. Soc. Symp. Proc.* **2010**, *1203*, 1203–J05−03.
(30) Michaelson, S.; Akhvlediani, R.; Hoffman, A.; Silverman, A.; Adler, J. *Phys. Status Solidi A* **2008**, *205*, 2099–2107.
(31) Berendsen, H. J. C.; Postma, J. P. M.; van Gunsteren, W. F.; DiNola, A.; Haak, J. R. *J. Chem. Phys.* **1984**, *81*, 3684–3690.
(32) Kátai, S.; Tass, Z.; Bori, L.; Hárs, G.; Deák, P. *Rev. Sci. Instrum.* **1999**, *70*, 3324–3328.
(33) Hagstrum, H. D. *Phys. Rev.* **1961**, *122*, 83–113.
(34) Brenner, D. W. *Phys. Rev. B* **1990**, *42*, 9458–9471.
(35) Eckert, M.; Neyts, E.; Bogaerts, A. *Chem. Vap. Deposition* **2008**, *14*, 213–223.
(36) May, P. W.; Harvey, J. N.; Smith, J. A.; Mankelevich, Y. A. *J. Appl. Phys.* **2006**, *99*, 104907.
(37) Robertson, J. *Mat. Sci. Eng. R* **2002**, *37*, 129–281.
(38) Lifshitz, Y.; Kasi, S. R.; Rabalais, J. W.; Eckstein, W. *Phys. Rev. B* **1990**, *41*, 10468–10480.